INSTITUTE OF PHYSICS PUBLISHING SUPERCONDUCTOR SCIENCE AND TECHNOLOGY

Supercond. Sci. Technol. **19** (2006) 934–940 doi:10.1088/0953-2048/19/9/009

Structure and microstructure of superconductor $Sr_2CuO_{3+\delta}$ (nominal $\delta = 0.4$) prepared under high pressure

H Yang, Q Q Liu, F Y Li, C Q Jin and R C Yu[1]

Laboratory for Extreme Condition Physics, Beijing National Laboratory for Condensed Matter Physics, Institute of Physics, PO Box 603, Beijing 100080, People's Republic of China

E-mail: rcyu@aphy.iphy.ac.cn

Received 6 April 2006, in final form 17 July 2006
Published 7 August 2006
Online at stacks.iop.org/SUST/19/934

Abstract

A *single-phase* superconductor $Sr_2CuO_{3+\delta}$ with nominal $\delta = 0.4$ (detected from x-ray powder diffraction (XRD) data) ($T_c = 75$ K) has been synthesized using a high-pressure technique. The structure and microstructure of this material have been carefully studied by means of transmission electron diffraction (ED), high-resolution transmission electron microscopy (HRTEM), electron energy-loss spectroscopy (EELS) and energy dispersive analysis of x-ray (EDX) techniques. Interestingly enough, ED and HRTEM investigations reveal that almost all grains of the tetragonal form $Sr_2CuO_{3+\delta}$ exhibit modulated features. This result strongly suggests that the superconductivity at 75 K in the material is associated with the modulated phases. Two types of modulated phases having different primitive cells but equal in volume are found in the sample. One is the face-centred orthorhombic modulated phase with a space group *Fmmm* and lattice constants of $\sim 5\sqrt{2}a_p \times 5\sqrt{2}a_p \times c_p$. The other is the base-centred monoclinic modulated phase with a space group $C2/m$ and unit-cell parameters of $a_m = 5\sqrt{2}a_p$, $b_m = c_p$, $c_m = \sqrt{26}\sqrt{2}/2a_p$ and $\beta = 101.3°$. The relative ratio of the former to the latter phase contents is about 4:1. Oxygen K absorption edges from EELS measurements suggest that the two modulated phases have the same hole intensity. Defects such as twin boundaries, small-angle asymmetrical tilt boundaries and dislocations are frequently observed in the $C2/m$ monoclinic modulated phase, and some of them are carefully studied by means of HRTEM, EELS and EDX.

1. Introduction

For the purpose of investigating the mechanism of superconductivity in high-T_c copper oxide superconductors, researchers usually prefer to use a simple system. The Sr–Cu–O system is such an ideal one having only two metallic elements, strontium and copper. In this system, superconductivity is displayed only in the high-pressure synthesized samples; however, a single-phase sample is difficult to obtain. In addition, modulated superstructures commonly exist in this system. Despite extensive studies on the Sr–Cu–O system, the origin of superconductivity in the high-pressure phase(s) of this simple system is still not clear, yet.

In 1993, Hiroi *et al* [1] first reported the occurrence of superconductivity at 70 K in $Sr_2CuO_{3+\delta}$ obtained using high-pressure techniques. They suggested that the main phase in this material is a highly apical oxygen-deficient K_2NiF_4-type tetragonal structure and the superconductivity results from this tetragonal phase. Later, several researchers also repeatedly observed the superconductivity at almost the same transition temperature of 70 K in the system synthesized under high pressures [2–4]. In all these high-pressure samples, the presence of modulated structures that have the K_2NiF_4-type tetragonal structure of $Sr_2CuO_{3+\delta}$ as their basic sub-

[1] Author to whom any correspondence should be addressed.

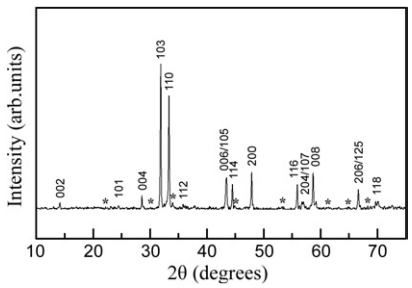

Figure 1. X-ray powder pattern of $Sr_2CuO_{3+\delta}$ with nominal $\delta = 0.4$. The weak peaks (indicated by the $*$) in the pattern are identified as the superstructure reflections.

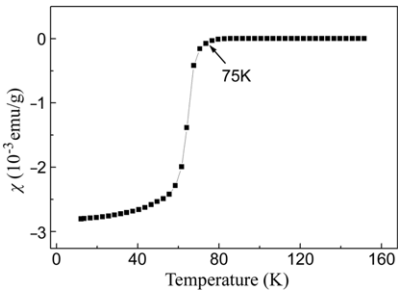

Figure 2. Temperature dependence of DC susceptibility (measured at an external magnetic field of 20 Oe) for $Sr_2CuO_{3+\delta}$ with nominal $\delta = 0.4$.

structure has been reported. For example, Hiroi *et al* [1] and Laffez *et al* [2] observed, separately, a $4\sqrt{2}a_p \times 4\sqrt{2}a_p \times c_p$ and a $5\sqrt{2}/2a_p \times 5\sqrt{2}/2a_p \times c_p$ modulated structure in their own samples, while Wang and Zhang *et al* [5, 6] reported a $5\sqrt{2}a_p \times 5\sqrt{2}a_p \times c_p$ structure in their samples. Contrary to the idea suggested in [1–3] that the non-modulated tetragonal form of $Sr_2CuO_{3+\delta}$ is the superconducting phase, Wang and Zhang *et al* [5, 6] suggested that the $5\sqrt{2}a_p \times 5\sqrt{2}a_p \times c_p$ modulated phase is actually responsible for the superconductivity. However, no convincing experimental results were given in all their works. In addition, the tetragonal form of $Sr_2CuO_{3+\delta}$ synthesized at ambient pressure, where modulated structures such as the $4\sqrt{2}a_p \times 4\sqrt{2}a_p \times c_p$ one were also found, has been shown to be isostructural with that obtained at high pressure on the basis of XRD analysis, but no superconductivity was observed in the ambient-pressure samples [7, 8]. The above works seem not to support the predication that the tetragonal form of $Sr_2CuO_{3+\delta}$ is responsible for the superconductivity. Shimakawa *et al* [9] studied the compounds of $Sr_2CuO_{3+\delta}$ synthesized at high pressure and ambient pressure separately by means of neutron diffraction, and suggested that the compounds prepared at different pressures both have an oxygen-deficient K_2NiF_4-type tetragonal structure with oxygen vacancies located in the Cu–O planes instead of the Sr–O layers. If the high-pressure tetragonal form is indeed superconducting, the neutron diffraction results will challenge the current understanding of superconductivity in the copper oxides, which is based on an oxygen vacancy-free Cu–O plane. Furthermore, Kawashima *et al* [10] reported that the superconducting phase with $T_c = 70$ K prepared from the nominal starting powders of Sr_2CuO_3 with $KClO_4$ oxidizer was not of 0201-type but of 0212-type Sr–Cu–O compound.

Up to now, it is still not clear what phase in the high-pressure material of $Sr_2CuO_{3+\delta}$ can lead to the superconductivity. In order to find the answer, recently we have undertaken a careful investigation on this system. In our work, focus is predominantly put on the synthesis of high-quality samples and the characterization of their structures and microstructures using transmission electron microscopy (TEM) characterizations. A single-phase K_2NiF_4-type tetragonal form of $Sr_2CuO_{3+\delta}$ (detected from x-ray powder diffraction (XRD) data) with nominal $\delta = 0.4$ ($T_c = 75$ K) was successfully synthesized by using a high-pressure technique. However, further investigations on the sample by electron diffraction (ED) and high-resolution transmission electron microscopy (HRTEM) revealed that almost all the grains of the $Sr_2CuO_{3+\delta}$ tetragonal form exhibit modulated features. Our TEM results strongly suggest that the superconductivity at 75 K observed in our high-pressure synthesized material of $Sr_2CuO_{3+\delta}$ with nominal $\delta = 0.4$ is associated with the modulated phases. In this paper, we mainly report these modulated phases and their defects studied by ED, HRTEM, electron energy-loss spectroscopy (EELS) and energy dispersive analysis of x-ray (EDX).

2. Experiments

To make the phase as pure as possible, we synthesized the $Sr_2CuO_{3+\delta}$ sample under high pressure using SrO_2 as an oxidizer. The starting material, Sr_2CuO_3, was prepared from high purity $SrCO_3$ and CuO raw materials mixed at a molar ratio of 2:1. The powder mixture was calcined at 950 °C for 24 h with several intermediate grindings. Then, Sr_2CuO_3, SrO_2, and CuO were mixed to yield the nominal composition $Sr_2CuO_{3+\delta}$ and subjected to high-pressure synthesis (6 GPa and 1100 °C for 1 h) using a cubic-anvil-type apparatus. More detailed process and discussion of the sample preparation will be reported elsewhere [11].

All the as-prepared samples were examined by XRD using Cu Kα radiation, and the results showed that the sample with nominal $\delta = 0.4$ appears to be of single phase. Figure 1 shows the XRD pattern of the $\delta = 0.4$ sample. All the main peaks in the pattern can be indexed in the K_2NiF_4-type tetragonal structure of $Sr_2CuO_{3+\delta}$ with lattice parameters $a = 0.38$ and $c = 1.25$ nm. The weak peaks (indicated by the $*$) visible in the pattern are identified as the superstructure reflections. We believe that so pure a high-pressure tetragonal form of $Sr_2CuO_{3+\delta}$ detected from XRD data has been obtained for the first time. The DC magnetic susceptibility measured on this sample with a SQUID magnetometer in an external magnetic field of 20 Oe revealed a superconducting transition temperature of 75 K (see figure 2). In the following, we focus on the TEM characterization of this sample and try to discuss the origin of the superconducting phase(s) in this system.

Thin foils for TEM studies were prepared by crushing the $Sr_2CuO_{3+\delta}$ in an agate mortar filled with alcohol, and then dispersing the fine fragments suspended in alcohol on a microgrid. A Tecnai F20 electron microscope with a field emission gun, installed at Beijing Laboratory of Electron Microscopy, Beijing National Laboratory for Condensed Matter Physics, was used for the TEM studies with an

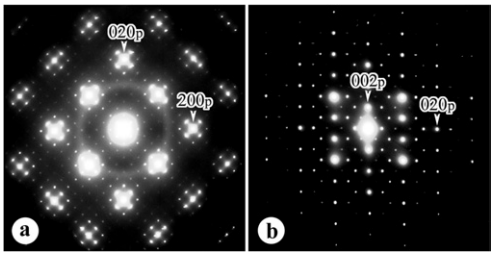

Figure 3. ED patterns of the *Fmmm* ($5\sqrt{2}a_p \times 5\sqrt{2}a_p \times c_p$) modulated phase taken along the (a) $[001]_p$ and (b) $[100]_p$ zone-axis directions.

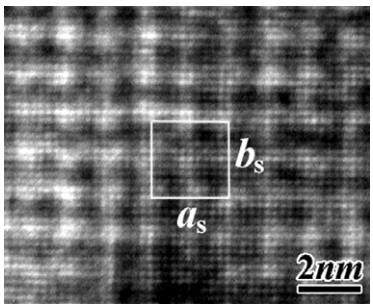

Figure 4. HRTEM image of the *Fmmm* modulated phase taken along the $[001]_p$ zone-axis direction. One unit cell is outlined by white solid lines.

acceleration voltage of 200 keV. EELS experiments were carried out in image mode, and the acquisition period of the spectra is 4 s. EDX measurements were performed under a spot size 11, and the acquisition period of the spectra is 30 s. Our previous TEM work on the 'apical oxygen doped' $Sr_2CuO_{2+\delta}Cl_{2-y}$ superconductor has suggested that an electron beam with high intensity could cause the superconductor to lose oxygen, and consequently result in the formation of modulated superstructure [12]. Therefore, during the TEM experiments, we tried our best not to expose the $Sr_2CuO_{3+\delta}$ sample to the intense electron beam, so as to avoid the electron-irradiation effects on the sample. For example, selected area electron diffraction (SAED) instead of convergent beam electron diffraction (CBED) has been used to search for and tilt grains. In fact, the $Sr_2CuO_{3+\delta}$ sample appeared to be stable under illumination with a weak electron beam. Even when the sample was exposed to the electron beam with high intensity, a short irradiation duration was not found to cause its structure change, either.

3. Results and discussion

The ED and HRTEM investigations show that almost all the grains in the sample exhibit modulated superstructures having the K_2NiF_4-type tetragonal structure of $Sr_2CuO_{3+\delta}$ as their basic sub-structure. The most common modulated phase in our sample exhibits a superlattice with a constant of $\sim 5\sqrt{2}a_p \times 5\sqrt{2}a_p \times c_p$ same as reported in [5] and [6]. Figures 3(a) and (b) show, respectively, the $[001]_p$ and $[100]_p$ zone-axis ED patterns of this modulated phase. Obviously, the superstructure modulation is two dimensional and the modulation plane lies in the a_pb_p-plane. This modulated structure can be characterized by two approximate wavevectors $a_s^* = (2\pi/a_p)(\frac{1}{10}, \frac{1}{10}, 0)$ and $b_s^* = (2\pi/a_p)(-\frac{1}{10}, \frac{1}{10}, 0)$, where the subscript '$s$' represents this type of modulated structure in this paper. Based on the consideration that the superstructure spots do not construct an exact tetragonal array but an orthorhombic one, and according to the extinction rule (*HKL* are all odd or all even), this modulated phase is identified to be a face-centred orthorhombic superstructure. Its space group can be approximately described as *Fmmm* in consideration of the sub-structure of the modulated phase being the K_2NiF_4-type tetragonal structure with the space group $I4/mmm$. The lattice parameters are $a_s \approx b_s = 5\sqrt{2}a_p$ and $c_s = c_p$. Figure 4 displays a HRTEM image of the *Fmmm* modulated phase taken along the $[001]_p$ zone-axis direction, showing clearly its modulated periodicity. One supercell is outlined in the square with white lines in the image.

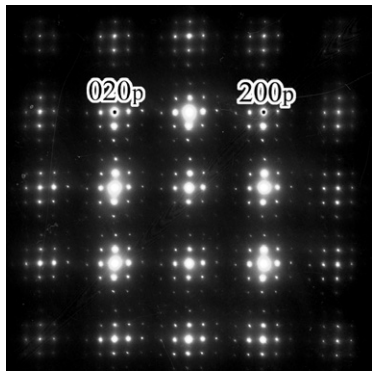

Figure 5. $[001]_p$ zone-axis ED pattern related to the *Fmmm* modulated phase, showing the two-dimensional modulation wavevectors a_s^* and b_s^* not exactly along the $[110]_p^*$ and $[\bar{1}10]_p^*$, respectively.

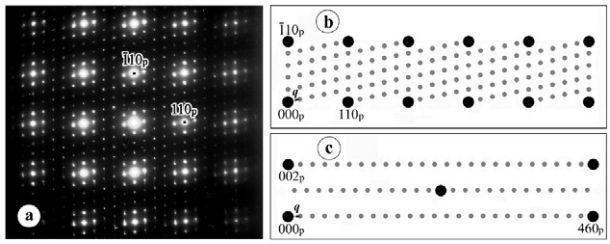

Figure 6. (a) ED pattern of the $C2/m$ modulated phase taken along the $[001]_p$ (or $[0\bar{1}0]_m$) zone axis. (b), (c) Schematic representations of the ED patterns along the $[001]_p$ (or $[0\bar{1}0]_m$) and $[3\bar{2}0]_p$ (or $[00\bar{1}]_m$) zone axes, respectively.

It should be noted that, in some grains related to the *Fmmm* modulated structure, the two-dimensional modulation wavevectors a_s^* and b_s^* are not exactly along the $[110]_p^*$ and $[\bar{1}10]_p^*$, respectively, but slightly inclined, as shown by an ED pattern in figure 5. The modulation wavevectors are rewritten as $a_s^* = (2\pi/a_p)(\frac{1}{10}(1+\varepsilon_1), \frac{1}{10}(1-\varepsilon_1), 0)$ and $b_s^* = (2\pi/a_p)(-\frac{1}{10}(1+\varepsilon_2), \frac{1}{10}(1-\varepsilon_2), 0)$, where $\varepsilon_1 \approx \varepsilon_2 \approx 0.05$.

In our sample, we found another new modulated phase. Figure 6(a) shows the $[001]_p$ zone-axis ED pattern of this modulated phase. By systemic tilting experiments the

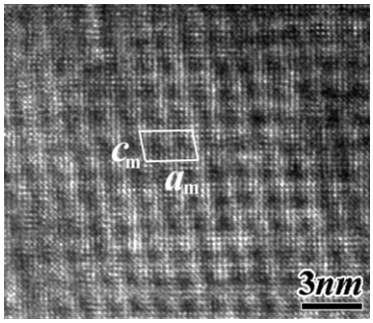

Figure 7. HRTEM image of the $C2/m$ modulated phase taken along the $[001]_p$ (or $[0\bar{1}0]_m$) zone-axis direction. One unit cell is outlined by white solid lines.

superstructure modulation is determined to be one dimensional and the modulation plane lies in the a_pb_p-plane. Two schematic representations of diffraction patterns along the $[001]_p$ and $[3\bar{2}0]_p$ directions, which can well reconstruct the reciprocal space of this modulated phase, are shown in figures 6(b) and (c), respectively. The superstructure peaks are characterized by a unique modulation wavevector $q = (2\pi/a_p)(\frac{2}{25}, \frac{3}{25}, 0)$. It is clear that the superlattice spots construct a base-centred monoclinic space array and the conditions for reflection are

$$HKL: H + K = 2n$$

$$H0L: H = 2n$$

$$0K0: K = 2n$$

where H, K and L represent the Miller indices of the monoclinic modulated phase. Since its sub-structure is the K_2NiF_4-type tetragonal structure with the space group $I4/mmm$, the monoclinic modulated phase has approximately a space group $C2/m$. The unit-cell parameters are $a_m = 5\sqrt{2}a_p$, $b_m = c_p$, $c_m = \sqrt{26}\sqrt{2}/2a_p$ and $\beta = 101.3°$, where the subscript 'm' represents the base-centred monoclinic modulated phase. Figure 7 shows an HRTEM image of the $C2/m$ modulated phase taken along the $[001]_p$ (or $[0\bar{1}0]_m$) zone-axis direction. One unit cell is outlined in the image by white solid lines. The HRTEM image, as well as the ED pattern in figure 6(a), indicates that the $C2/m$ modulated phase has a primitive cell equal to that of the *Fmmm* modulated phase in volume. The $C2/m$ modulated phase is also commonly found in our sample. An attempt has been made to evaluate the relative content of the two types of modulated phases, although the TEM results usually suffer from poor statistics due to the observation of a limited number of individual grains. In our evaluation, we conclude, by observing 50 grains, that about 20% of the grains have the $C2/m$ modulated structure, and the rest exhibit the *Fmmm* modulated structure.

In the $C2/m$ monoclinic modulated phase, defects such as twin boundaries, asymmetrical tilt boundaries (ATBs) and dislocations are observed frequently.

A typical twin boundary observed in the $C2/m$ monoclinic modulated phase is the $\Sigma5(001)_m$ (or $\Sigma5(\bar{1}10)_p$) twin boundary. Figure 8(a) shows, as an example, an

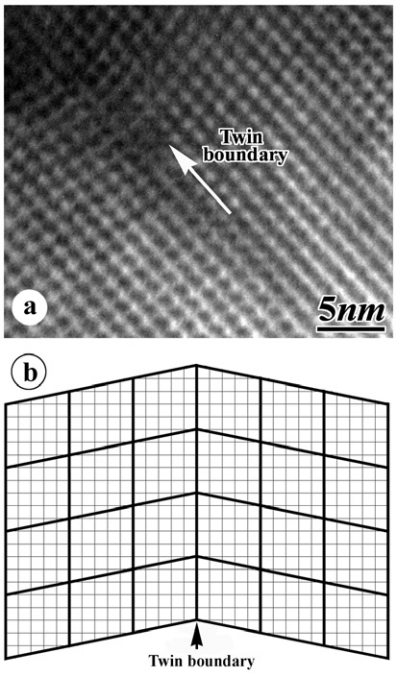

Figure 8. (a) HRTEM image of a $\Sigma5(001)_m$ (or $\Sigma5(\bar{1}10)_p$) twin boundary in the $C2/m$ monoclinic modulated phase. (b) A schematic diagram of the twin boundary. In the schematic diagram the thick linear latticework represents the monoclinic modulated structure while the thin linear latticework represents the basic K_2NiF_4-type tetragonal structure of $Sr_2CuO_{3+\delta}$.

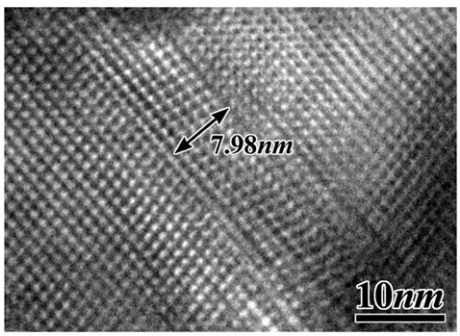

Figure 9. HRTEM image of a twin slab in the monoclinic modulated phase. The width of the twin slab is about $15\sqrt{2}a_p$ (7.98 nm).

HRTEM image of the twin boundary. It should be noted that the twinning results only from the changes of modulation, while the basic sub-structure keeps the 'perfect' K_2NiF_4-type tetragonal structure. A schematic diagram of the twin boundary is shown in figure 8(b), clearly displaying the features of the twinning. Such a modulated twinning can be expected, since the basic tetragonal structure of $Sr_2CuO_{3+\delta}$ can provide a pair of equivalent wavevectors $q_1 = (2\pi/a_p)(\frac{2}{25}, \frac{3}{25}, 0)$ and $q_2 = (2\pi/a_p)(\frac{3}{25}, \frac{2}{25}, 0)$ for the monoclinic modulation. Figure 9 shows the HRTEM image of a pair of parallel twin boundaries. The width of the twin slab is about $15\sqrt{2}a_p$ (7.98 nm).

Another type of grain boundary observed in the monoclinic modulated phase is the small-angle ATB. One of

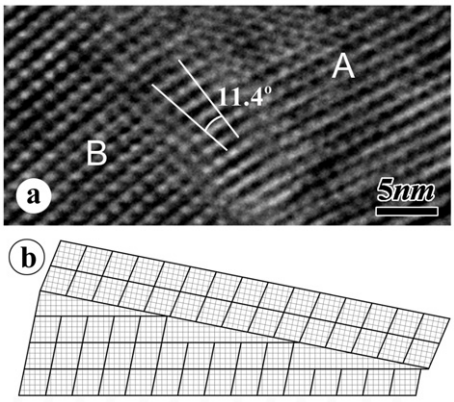

Figure 10. (a) HRTEM image of an 11.4° small-angle ATB. (b) The schematic representation of the grain boundary constructed from (a). The small-angle ATB results from the asymmetrical tilt of the sub-structure of the monoclinic modulated phase.

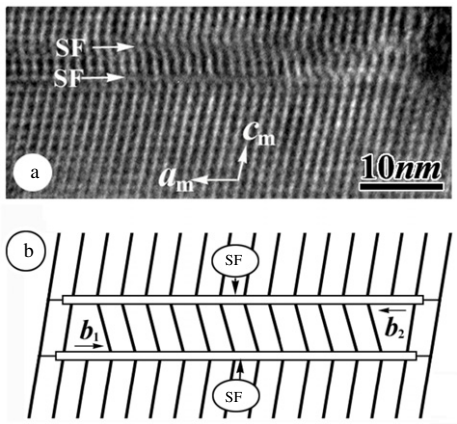

Figure 11. (a) HRTEM image of a dislocation dipole. (b) The corresponding schematic representation of the dipole. The stacking faults resulting from the dislocations are clearly seen in the image, and schematically shown in (b). It should be stressed that the dislocations and the stacking faults resulting from them are merely produced by the changes of local modulation, while their sub-structure keeps the 'perfect' K_2NiF_4-type tetragonal structure.

the characteristics of the small-angle ATB is that the basal planes of one grain are macroscopically parallel to the grain boundary plane. Figure 10(a) shows the HRTEM image of an 11.4° ATB, taking the $a_m b_m$-plane (or $(\bar{1}10)_p$ plane) of grain A as the grain boundary plane. Different from the twin boundary arising from only superstructure modulation, the small-angle ATB results from asymmetrical tilt of the sub-structure of the monoclinic modulated phase. Figure 10(b) shows the schematic representation of the grain boundary constructed from figure 10(a). Generally, the modulated structure at the parallel side of the small-angle ATB keeps good periodicity, although the basic lattices near the boundary are slightly distorted due to the asymmetrical tilt of the sub-structure. At the inclined side of the boundary, the monoclinic modulated periodicity usually suffers from changes near the boundary.

Dislocations are also found to be the common defects in the monoclinic modulated phase. One kind of the dislocations is the $\frac{1}{2}a_m\langle 100\rangle_m$ edge dislocation, taking the

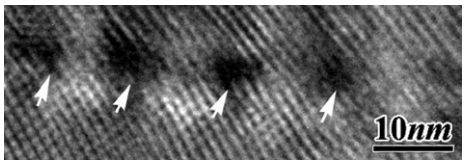

Figure 12. HRTEM image of an array of dislocation cores with a periodic separation of about 12.5 nm.

$(001)_m$ plane as the glide plane and with the dislocation line along $\langle 010\rangle_m$. These dislocations are seen to appear generally in pairs and form dipoles. Figure 11(a) shows the HRTEM image of such a dislocation dipole. The corresponding schematic representation of the dislocation dipole is shown in figure 11(b). Assuming that Burgers circuits are taken counterclockwise, the counter-oriented Burgers vectors $\boldsymbol{b}_1$ and $\boldsymbol{b}_2$ of the two dislocations, as indicated in the schematic diagram, will be $\frac{1}{2}a_m[\bar{1}00]_m$ and $\frac{1}{2}a_m[100]_m$, respectively. The dislocations usually result in the formation of stacking faults on their glide plane, which is clearly seen from the HRTEM image in figure 11(a). One point should be stressed that the dislocations and the stacking faults resulting from them are merely produced by the changes of local modulations, while the sub-structure keeps the 'perfect' K_2NiF_4-type tetragonal structure of $Sr_2CuO_{3+\delta}$. This phenomenon can be observed more clearly by HRTEM for the superconductor $(Sr, Ca)_2CuO_{2+\delta}Cl_{2-y}$ (our work) and the details will be reported later [13].

Figure 12 shows the HRTEM image of an array of dislocation cores with a periodic separation of about 12.5 nm. These dislocation cores are composed of a possible combination of screw and edge dislocations. In general, there is a distortion in the lattice of the sub-structure around the dislocation cores. If the $C2/m$ modulated phase is superconducting, the defects observed in its structure will play important roles in the properties of the superconductor; in particular, they can act as flux pinning centres to enhance the critical current density J_c.

The *Fmmm* and $C2/m$ modulated phases were also studied by means of EELS. For the hole doped copper oxides, the oxygen K edge fine structure can provide important information about the charge carriers and their crystallographic confinement [14, 15], and the presence of an pre-peak on the low-energy part (usually $E < 531$ eV) of the oxygen K edge is related to the unoccupied O 2p states. The intensity of the pre-peak is proportional to the number of holes introduced by doping. Curves (a) and (b) in figure 13 show the oxygen K absorption edges obtained from the 'perfect' areas of the *Fmmm* and $C2/m$ modulated phases, respectively. The shapes of the two EELS spectra are similar; in particular, the pre-peak at ~528 eV has the same intensity. The pre-peak, which is also clearly observed for the newly synthesized Cl-0201-type superconductor [16], is attributed to transitions from the O 1s core state into doped unoccupied O 2p states near E_F. A similar hole-related pre-peak for the *Fmmm* and $C2/m$ modulated phases indicates that a similar hole intensity was doped in them. Oxygen K absorption edges for some defect domains of the $C2/m$ monoclinic modulated phase were also measured. The dislocation cores shown in figure 12 are found to be hole

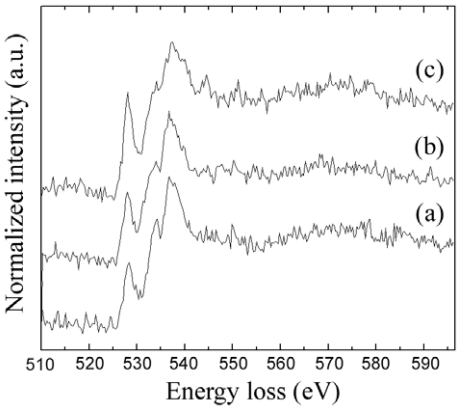

Figure 13. Oxygen K absorption edges measured by EELS. (a), (b) Oxygen K edges obtained, respectively, from 'perfect' areas of the *Fmmm* and $C2/m$ modulated phases, showing a similar hole-related pre-peak. (c) Oxygen K edge from a dislocation core domain in the monoclinic modulated phase, showing a much higher hole-related pre-peak.

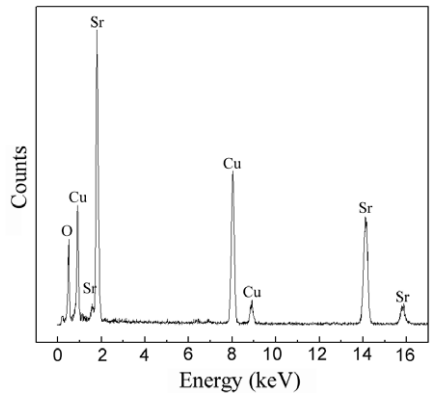

Figure 14. EDX chart for a dislocation core domain. Composition quantification from the chart suggests Sr:Cu < 2:1.

rich. As an example, curve (c) in figure 13 shows the oxygen K edge obtained from one of the dislocation cores, where a much higher hole-related pre-peak is clearly seen. The hole richness in the defect domains can be explained by the Sr deficiency. Composition analysis by EDX (figure 14 shows a typical EDX chart for a dislocation core) suggests Sr:Cu < 2:1.

Based on the ED and HRTEM investigations, the high-pressure synthesized superconducting material $Sr_2CuO_{3+\delta}$ with nominal $\delta = 0.4$ was identified to contain two types of modulated phases, i.e. *Fmmm* and $C2/m$ modulated phases. Now other questions arise: What results in the formations of the two modulated phases? Are the mechanisms resulting in them the same? Which one of them is responsible for the 75 K superconductivity?

Zhang *et al* [6] proposed an atomic model of the average commensurate lattice to explain the *Fmmm* ($5\sqrt{2}a_p \times 5\sqrt{2}a_p \times c_p$) modulated structure. They suggested that the modulated structure results from metal ion shear displacements with half sine and half cosine waves along $\langle 110 \rangle_p$ directions. According to this model, the Cu ions have a half cosine wave displacement while Sr ions have a half sine wave displacement, indicating that oxygen atoms are lost in the Cu–O planes instead of in the Sr–O layers. If this model is valid, the *Fmmm* modulated phase would not be the superconducting one according to our current understanding of superconductivity in the copper oxides, which is based on oxygen vacancy-free Cu–O planes. Then the 75 K superconductivity observed in our sample would be ascribed to the $C2/m$ modulated phase. If the $C2/m$ modulated phase is indeed the superconducting one, then the oxygen vacancies will be reasonably located in the Sr–O layers, and the formation of the $C2/m$ modulated structure is naturally explained to be the ordering of the apical oxygen vacancies. The mechanisms resulting in the two modulated phases and which phase the superconductivity comes from will be determined by further experiments and this work is under way.

4. Conclusions

The structure and microstructure of the single-phase (from XRD data) superconducting material $Sr_2CuO_{3+\delta}$ with nominal $\delta = 0.4$ obtained by the high-pressure technique have been studied by means of ED, HRTEM, EELS and EDX. The results obtained can be summarized as follows.

(1) The ED and HRTEM investigations show that almost all the grains exhibit modulated structures having the K_2NiF_4-type tetragonal structure of $Sr_2CuO_{3+\delta}$ as their sub-structure, which strongly indicates that the superconductivity at 75 K in the material is associated with the modulated phases.

(2) Two types of modulated phases having different primitive cells but equal in volume are found in the material. One is the face-centred orthorhombic modulated phase (space group *Fmmm*) with a lattice constant of $\sim 5\sqrt{2}a_p \times 5\sqrt{2}a_p \times c_p$. The other is the base-centred monoclinic modulated phase (space group $C2/m$) with unit-cell parameters of $a_m = 5\sqrt{2}a_p$, $b_m = c_p$, $c_m = \sqrt{26}\sqrt{2}/2a_p$ and $\beta = 101.3°$. The relative ratio of the two phase contents is about 4:1.

(3) Oxygen K absorption edges from EELS measurements suggest that the two modulated phases have the same hole intensity.

(4) In some grains showing the *Fmmm* modulated structure, the two-dimensional modulation wavevectors a_s^* and b_s^* are not exactly along the $[110]_p^*$ and $[\bar{1}10]_p^*$, respectively, but slightly inclined. The modulation wavevectors can be rewritten as $a_s^* = (2\pi/a_p)(\frac{1}{10}(1+\varepsilon_1), \frac{1}{10}(1-\varepsilon_1), 0)$ and $b_s^* = (2\pi/a_p)(-\frac{1}{10}(1+\varepsilon_2), \frac{1}{10}(1-\varepsilon_2), 0)$, where $\varepsilon_1 \approx \varepsilon_2 \approx 0.05$.

(5) Defects such as twin boundaries, asymmetrical tilt boundaries and dislocations are frequently observed in the $C2/m$ modulated phase. The $\Sigma 5(001)_m$ twin boundary and the $\pm a_m/2[100]_m$ dislocation dipole result from the changes of modulation, while their sub-structure keeps the 'perfect' K_2NiF_4-type tetragonal structure of $Sr_2CuO_{3+\delta}$. The small-angle ATB arises from asymmetrical tilt of the sub-structure. The observed dislocation cores are composed of a possible combination of screw and edge dislocations, and are found to be hole rich by the O K

EELS results. Composition analysis from EDX suggests that the high hole intensity in the cores results from Sr deficiency.

Acknowledgments

This work was supported by the National Natural Science Foundation of China (grant Nos 50471053, 50321101, 50332020 and 5041009) and the State Key Development Program for Basic Research of China (grant Nos 2005CB623602 and 2005CB724402).

References

[1] Hiroi Z, Takano M, Azuma M and Takeda Y 1993 *Nature* **364** 315
[2] Laffez P, Wu X J, Adachi S, Yamauchi H and Môri N 1993 *Physica* C **222** 303
[3] Han P D, Chang L and Payne D A 1994 *Physica* C **228** 129
[4] Shimakawa Y, Jorgensen J D, Mitchell J F, Hunter B A, Shaked H, Hinks D G, Hitterman R L, Hiroi Z and Takano M 1994 *Physica* C **228** 73
[5] Wang Y Y, Zhang H, Dravid V P, Marks L D, Han P D and Payne D A 1995 *Physica* C **255** 247
[6] Zhang H, Wang Y Y, Marks L D, Dravid V P, Han P D and Payne D A 1995 *Physica* C **255** 257
[7] Mitchell J F, Hinks D G and Wagner J L 1994 *Physica* C **227** 279
[8] Bonvalot M, Beaugnon E, Bourgault D, Núñez-Regueiro M and Tournier R 1997 *Physica* C **282–287** 539
[9] Shimakawa Y, Jorgensen J D, Mitchell J F, Hunter B A, Shaked H, Hinks D G, Hitterman R L, Hiroi Z and Takano M 1994 *Physica* C **228** 73
[10] Kawashima T and Takayama-Muromachi E 1996 *Physica* C **267** 106
[11] Liu Q Q *et al* 2006 at press
[12] Yang H, Liu Q Q, Li F Y, Jin C Q and Yu R C 2005 *Supercond. Sci. Technol.* **18** 1360
[13] Yang H *et al* 2006 at press
[14] Romberg H, Nücker N, Alexander M, Fink J, Hahn D, Zetterer T, Otto H H and Renk K F 1990 *Phys. Rev.* B **41** 2609
[15] Nücker N, Romberg H, Xi X X, Fink J, Gegenheimer B and Zhao Z X 1989 *Phys. Rev.* B **39** 6619
[16] Yang H, Liu Q Q, Yu R C, Li F Y and Jin C Q 2005 *Supercond. Sci. Technol.* **18** 813